Angle-resolved photoemission and its current applications in surface science

Yong Q. Cai

Japan Science and Technology Corporation, and
Institute for Solid State Physics, University of Tokyo

Angle-resolved photoemission has proven to be a powerful tool, especially in combination with polarized, tunable light produced by synchrotron radiation, for the study of the electronic structure of a wide range of materials. Its intrinsic surface sensitivity makes it an ideal choice for addressing some issues of current interest in surface science, among which are the electronic structure of metal-oxide thin films and the effects of electron-phonon interaction in simple, two-dimensional metallic systems. After a brief introduction of the technique of angle-resolved photoemission and the properties of synchrotron radiation, examples are given to illustrate some current activities in these areas. In particular, the electronic structure of an iron-oxide thin film, namely, $Fe_3O_4(111)$ epitaxially grown on Pt(111), and the effects of strong electron-phonon interaction on α-Ga(010) surface and its link with a phase transition on the surface will be described and discussed.

I. INTRODUCTION

Photoemission[1] is conceptually a simple process in which one observes the emission of electrons from matter in response to incident radiation. A typical modern angle-resolved photoemission (ARP) experiment [see Fig. 1(a)] involves therefore the incidence of monochromatic radiation onto a sample and the measurement of the angular (momentum) and energy distribution of the photoelectrons. The use of synchrotron radiation[2] as a light source enriches the way in which ARP experiments can be performed. Such radiation is produced by fast-moving ($\beta = v/c \approx 1$) electrons in a circular orbit. The light is intrinsically polarized in the plane of the orbit and can be monochromatized by gratings that allow the energy to be tuned over a wide range. One may, for example, sweep the photon energy while keeping the kinetic energy fixed during an ARP experiment. The spectral variations obtained will emphasize initial-state density effects [i.e., the so-called constant-final-state mode]. If the kinetic energy and the photon energy are varied simultaneously, transitions from a fixed initial state are measured, so the spectra reflect mainly the density variation of the final states [the constant-initial-state mode]. Polarization and the angle of incidence of the light may be used in a similar way to study, for example, the transition selection rules or to increase surface sensitivity.[3] The spin of the emitted electrons can also be utilized in a spin-resolved experiment to obtain important information on magnetic properties.[4]

In principle, the kinetic energy (E_{kin}) of the photoelectrons with respect to the vacuum level (E_{vac}) of the spectrometer is measured. The initial-state energy (E_i) of the electron is then inferred based on the following energy conservation relation:

$$E_i = E_{kin} + E_{vac} - \hbar\omega, \tag{1}$$

where E_i and E_{vac} are both relative to the Fermi level (E_F). In practice, particularly for metallic systems, E_i is more conveniently measured directly from the spectra since the position of the Fermi level is known experimentally [see Fig. 1(b)]. For semiconductors, it is more common to

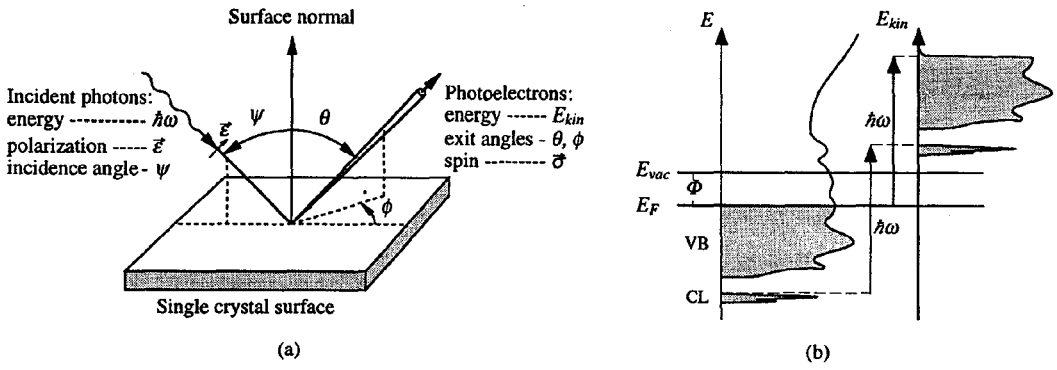

FIG. 1. (a) A schematic illustration of, and (b) the energy relation in an angle-resolved photoemission experiment.

refer to the valence band maximum, although the position of which is not always well defined.[3] Insulators present additional problems unless the effect of electrostatic charging is circumvented (see Sec. II). Since the excitation leaves a hole behind, it is important to realize that the energy so obtained is the difference in total energy between the original N-electron system and the remaining one with $(N-1)$ electrons, and should therefore be regarded only as the energy of an excited, quasiparticle state.[3]

On the other hand, due to the breaking of the periodicity along the surface normal direction, only the component of the wave vector parallel to the surface is conserved following the emission of the photoelectrons from the solid:

$$\mathbf{k}^{\parallel} = \mathbf{K}^{\parallel} \pm \mathbf{g}, \tag{2}$$

where $\mathbf{g}$ is a surface reciprocal lattice vector, and $\mathbf{k}^{\parallel}$ and $\mathbf{K}^{\parallel}$ are the wave vector inside and outside the solid, respectively. The magnitude of $\mathbf{K}^{\parallel}$ can be obtained from E_{kin} and the emission polar angle θ through:

$$K^{\parallel} = \frac{\sqrt{2mE_{kin}}}{\hbar} \sin\theta, \tag{3}$$

and therefore $\mathbf{k}^{\parallel}$ can be inferred. Together with the surface sensitivity offered by the finite escape depth of the photoelectrons,[3] this makes angle-resolved photoemission an ideal tool for investigating the electronic structure of 2D systems, for which $\mathbf{k}^{\parallel}$ is the only good quantum number. For the component perpendicular to the surface ($k^{\perp}$), however, no corresponding relation of conservation exists. To completely determine the wave vector of 3D, bulk electronic states in angle-resolved photoemission, additional effort must hence be made. For that purpose, two approaches have been pursued.[3] One involves an assumption about the final states involved in the optical transition step of the three-step model[3] using, e.g., the so-called free-electron final states, or a calculated band structure. The other takes advantage of some special properties of photoemission, a good representative of which has been the energy coincidence (or triangulation) method.[3] The former approach is more commonly used and will be illustrated in Sec. II, in which a study of the valence electronic structure of an epitaxial $Fe_3O_4(111)$ thin film will be described. In Sec. III, an example will be presented of a 2D electronic system, namely the surface electronic structure of α-Ga(010) that shows strong electron-phonon coupling effects.

II. VALENCE-BAND STRUCTURE OF A FE_3O_4(111) FILM

The motivation to study the iron oxide thin film stems from the fact that, despite the crucial role played by the surfaces of metal oxides in many of the applications of these technologically important materials, little is known about their atomic and electronic structure as compared to those of metals and semiconductors.[5] The central problem responsible for this state of affairs lies in the difficulty in the preparation of well-defined surfaces of metal oxides for surface science studies. Their brittle nature and the difficulty in maintaining the oxygen concentration during conventional cleaning processes of bulk single-crystal surfaces in ultrahigh vacuum often lead to disordered and/or non-stoichiometric surfaces. In contrast, the recent development of growing single-crystal metal-oxide thin films epitaxially on conducting substrates appears to have solved these problems.[6] The cleanliness, stoichiometry and crystalline order of the surface of these thin oxide films can be well controlled, and yet structurally and chemically they are found to be identical with their bulk counterparts.[6,7] Furthermore, for insulating oxides the electrostatic charges caused by analytical techniques involving the use of charged particles can be dissipated via the conducting substrate. These oxide thin films therefore provide a new playground for spectroscopic and microscopic studies of the electronic and atomic structures of metal oxides, which is a prerequisite for understanding the physical principles governing their rich electrical and magnetic properties.[8]

For iron oxides, it has been shown that well-ordered Fe_3O_4(111) films can be prepared epitaxially on clean Pt(111) surfaces.[7] The film is grown by repeated cycles of iron deposition and subsequent oxidation in a 1×10^{-6}-mbar oxygen partial pressure at a temperature between 600 – 730 °C. A thorough scanning tunnelling microscopy (STM) investigation has found that the iron oxide grows layer by layer in the FeO structure up to 2 monolayers; afterward, Fe_3O_4(111) islands begin to form and eventually coalesce to give a thick film.[9] X-ray photoelectron and Auger electron spectroscopy studies[10,11] of this oxide film have confirmed the Fe_3O_4 stoichiometry, and a dynamic low-energy-electron diffraction (LEED) intensity analysis[11] has shown the surface to be a strongly relaxed, unreconstructed Fe_3O_4(111) surface.

The electronic and magnetic properties of Fe_3O_4 (magnetite) have been studied intensively over the years. Fe_3O_4 is a ferrimagnet with the cubic inverse spinel structure.[8] Two cation sites exist in the crystal: One site designated *A* is tetrahedrally coordinated to oxygen and is occupied only by Fe^{3+} ions. The other site designated *B* is octahedrally coordinated to oxygen and is occupied by equal numbers of Fe^{2+} and Fe^{3+} ions. At about 120 K (T_v), magnetite undergoes a phase transition, named after Verwey,[12] in which the conductivity drops sharply by two orders of magnitude[8] and the crystallographic structure changes from cubic to monoclinic.[13] The high electrical conductivity of magnetite at room temperature is attributed to electron hopping between the Fe^{2+} and the Fe^{3+} ions occupying the *B* site by theories based on the localized-electron point of view. The Verwey transition freezes these electrons and causes an ordering of the extra electron (compared to Fe^{3+}) at the Fe^{2+} *B* site at temperatures below T_v, although the precise ordering is still unclear.[14] The same phenomenon, however, can also be explained from band theory which considers the high conductivity as a natural consequence of the half-filled 3*d* band of iron atoms located at the *B* site. The Verwey transition is a result of a band splitting due to the increasing importance of electron-electron correlation and/or electron-phonon interactions at low temperatures.[8]

Our angle-resolved photoemission study on the Fe_3O_4(111) thin film supports the band-theory description of the electronic structure of magnetite.[15] In Fig. 2 the normal emission spectra of the valence band region at room temperature (300 K) are shown. The spectra are collected

in the photon energy range of 40 – 80 eV, which includes the Fe $3p \rightarrow 3d$ excitation threshold at 56 eV where strong resonant enhancement of photoemission is seen. The Fermi level corresponds to that of the platinum substrate. The film thickness is estimated to be about 60 Å, in which case the influence of the platinum substrate on the spectra is diminishingly small. There is finite photoemission intensity at the Fermi level in all spectra, which is clearly due to the feature at the lowest binding energy and is compatible with the high conductivity of magnetite seen for bulk single crystals.[16,17] Clear dispersion of several distinct features can be seen in Fig. 2. This is attributed to the higher surface quality of the iron oxide film compared to the cleaved surfaces where the k-smearing caused by surface roughness is less of a problem.

One can examine in detail the observed valence-band structure by comparing with first-principles calculations. This is carried out using the so-called structure plot in which both the experimental data points and calculated transition lines are shown (Fig. 3). Here, the data points are peak or shoulder positions in the spectra determined from the local minima positions in the second derivative of the smoothed spectra. Solid lines represent direct transitions satisfying:[3]

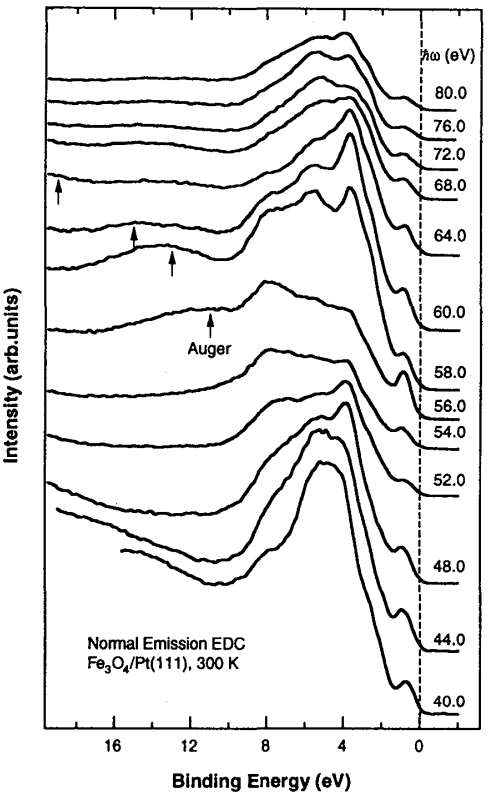

FIG. 2. Valence-band normal-emission spectra from the $Fe_3O_4(111)$ film taken at room temperature (300 K). From Ref. 15.

$$\hbar\omega = E_f(\mathbf{k}) - E_i(\mathbf{k}), \tag{4}$$

where the initial states (E_i) are the band structure along the ΓL symmetry line calculated recently by Yanase and Hamada.[18] The final states (E_f) are free-electron final states of the form:

$$E_f(\mathbf{k}) = \frac{\hbar^2}{2m}(\mathbf{k} + \mathbf{G})^2 - E_0, \tag{5}$$

where E_0 is the inner potential with respect to the Fermi level, and $\mathbf{G}$ a bulk reciprocal lattice vector. Only the primary cone[3] is used here. In order to produce the match shown in Fig. 3, a value of 13.0 eV has been used for E_0. The calculated valence bands have also been shifted to higher binding energies by 0.2 eV. The transition lines calculated using the majority and minority spin bands are shown separately for clarity in the left and right panels, respectively.

For the feature at ≤ 0.9 eV binding energy good agreement is found with the minority (spin-down) transitions at photon energies between 40 – 53 eV. In fact this is the only possible fit since the spin polarization has been found to be negative from the Fermi level down to approximately 1.7 eV at 200 K by spin-polarized photoemission.[19] Its dispersion shows a clear maximum in binding energy at around 46 eV photon energy and therefore it is identified as emission from the Γ point. The other critical point L in the symmetry line, as well as the wave vector (k) of all the other data points, are then fixed by the calculation.

A more careful examination of the spectra in this region, as shown in Fig. 4, reveals that two bands, derived from a peak and a shoulder, are in fact present in the spectra. The two bands thus appear to correspond to the first two occupied minority-spin bands in the calculation, both of which disperse upward towards the zone boundary. Although in absolute energy terms there is still up to 0.4 eV difference between the experiment and the calculation in the critical-point energies,[15] the observation of these lowest binding energy features and of the finite intensity at the Fermi level firmly establishes the metallic nature of magnetite and indicates that magnetite should be treated with band theory.

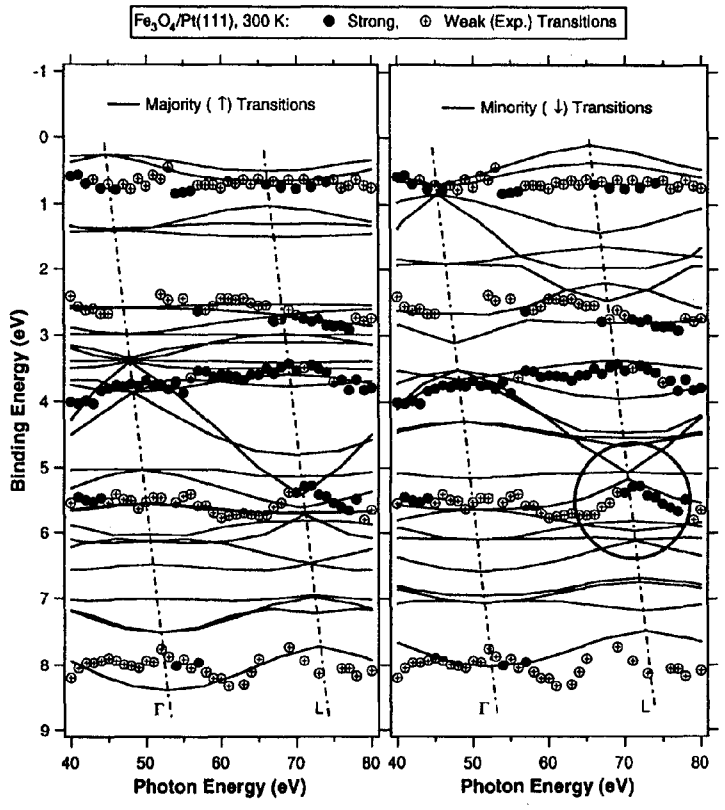

FIG. 3. Structure plot for normal emission data taken at 300 K. Refer to the text for details. From Ref. 15.

Agreement for the rest of the data is less obvious. While the weak transitions are found to be associated equally well with both the majority- and minority-spin bands, the strong features appear to agree better with the minority-spin transitions. This is particularly true for the strong feature around 4.0 eV for $\hbar\omega < 56$ eV and that around 5.5 eV for $\hbar\omega > 70$ eV. These two features appear to be parts of the same calculated band which disperses downward from 3.5 eV at Γ to about 5.0 eV at the zone boundary L, where a small gap opens. It then extends into the next zone and disperses to 5.5 eV at $\hbar\omega =$ 80 eV. The gap is not visible in the experimental data, but the band folding at the zone boundary (circled in Fig. 3) can be seen. Alternatively, a nearby majority-spin band with similar dispersion may also be assigned to these strong transitions. The energies, however, differ substantially more from those in the experiments. The comparison therefore favors the minority-spin band assignment. Since the thin film was not magnetized throughout its preparation, it is unlikely that this apparently better agreement is due to a preferential domain orientation. The problem may simply be due to some inaccuracy in the calculated band energies.[15] These features

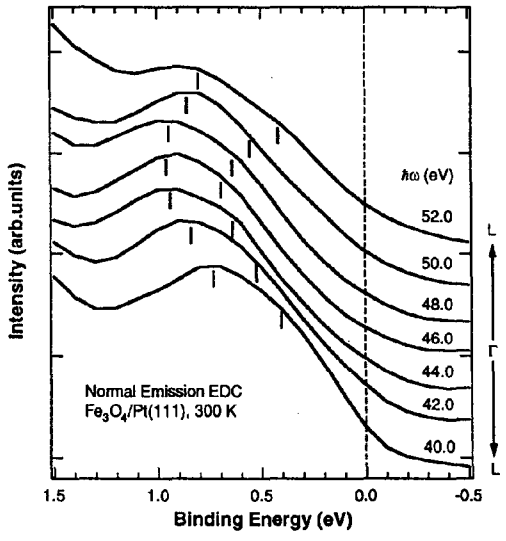

FIG. 4. Spectra taken at 300 K showing the dispersion of the lowest binding energy features (indicated by the vertical bars). From Ref. 15.

may therefore contain contributions from both the majority- and minority-spin bands, a precise identification of which can only be achieved in spin-resolved ARP experiments.

Changes to the photoemission spectra associated with the Verwey transition have also been investigated by taking data at 90 K and are found to be quite subtle. The data has been analyzed in the same way as that at 300 K. The results are shown in Fig. 5. No appreciable changes are observed in the spectral region near the Fermi edge within the range of photon energies used. Chainani *et al.*[20] have, however, reported photoemission experiments on cleaved $Fe_3O_4(110)$ surfaces and found a downwards shift of about 70 meV of the Fermi edge when their sample was cooled from 300 K to 100 K, consistent with the characteristics of the Verwey transition. In principle, one would expect the opening up of a band gap at the point where the first minority-spin band in the high temperature phase is expected to cross the Fermi level in order to explain the Verwey transition from the band structure point of view. Following the dispersion observed in Fig. 4, a crossing should occur at a $\hbar\omega < 40$ or > 54 eV. However, due to the lack of data at photon energies < 40 eV and to the interference of resonant photoemission at photon energies > 54 eV (see below), the above possibility was not confirmed. Nevertheless, an interesting difference can be seen within the circled regions in Figs. 3 and 5. In the data taken at 300 K, as stated above, folded transitions from the zone boundary L are present, whereas at 90 K no such band folding is observed. The absence of folded transitions at the lower temperature is consistent with the change of the crystallographic symmetry associated with the Verwey transition:[13] the L point is no longer a Brillouin zone boundary of the monoclinic structure at low temperature.

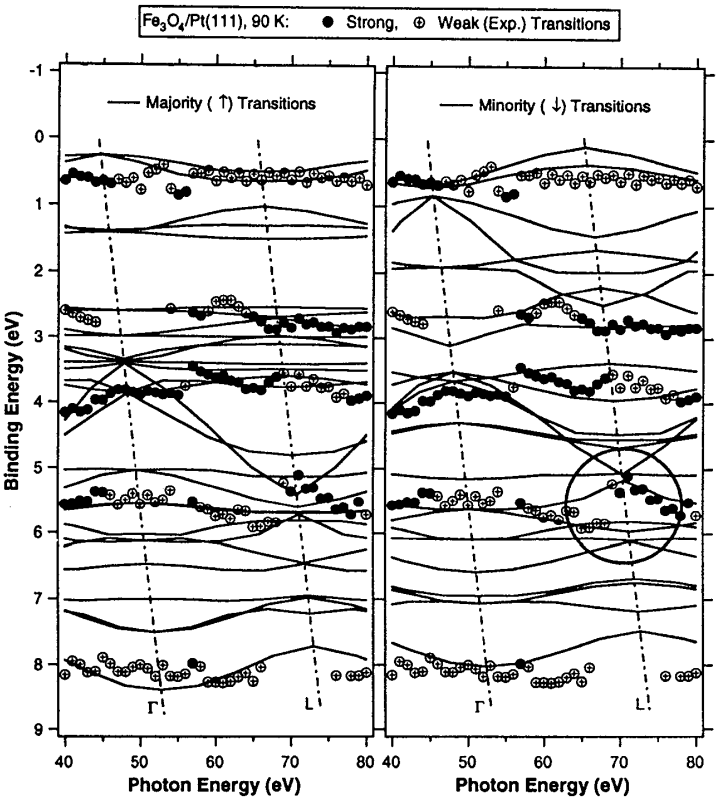

FIG. 5. Structure plot for data taken at 90 K. From Ref. 15.

The band dispersion discussed above is strongly interrupted by the resonant photoemission across the Fe $3p \rightarrow 3d$ excitation threshold at 56 eV, particularly of those Fe $3d$-derived bands above 4 eV binding energies. The mechanism of resonant photoemission in $3d$ transition metals and their compounds is well known.[21] For iron oxides and other late transition-metal oxides, it is generally believed that the $3p \rightarrow 3d$ excitations are quite localized and involve only $3d$-derived states. This may therefore explain the above observation that mainly the dispersion of Fe $3d$-derived bands is affected by the resonant photoemission.

The resonant behavior of the final states involved in the resonant photoemission has also been investigated and found to be in essential agreement with previous resonant photoemission studies of $Fe_3O_4(110)$ by Lad and Henrich.[17] It should, however, be pointed out that the bind-

ing energies of the resonating states are somewhat different from the values obtained for the $Fe_3O_4(111)$ film. These differences have been attributed to crystal anisotropy and band structure effects.[15] This is because the resonant photoemission involves direct photoemission from the $3d$ levels which is determined by the initial- and final-state band structures, and despite the Coulomb interaction in the Auger decay the wave vector remains a good quantum number.

Finally, no changes have been observed in the resonant behavior as the temperature is lowered to 90 K,[15] indicating that the Verwey transition does not change the nature of the final states involved in the resonant photoemission. This demonstrates that resonant photoemission is indeed a localized process on which neither a charge ordering at the cation B site nor crystallographic symmetry variations would have any noticeable effect.

III. ELECTRON-PHONON INTERACTION ON α-GA(010)

α-gallium is one of those semi-metals that not only have a low density of states at the Fermi level, but also support electronic states on their surfaces which cross E_F and render the surface much more metallic than the bulk.[22,23] Hence, these surfaces provide the opportunity for investigating the properties of quasi two-dimensional metals. The motivation for the work presented here is to study the effects of electron-phonon interaction on the electronic dispersion of a two-dimensional metal.[24] Although this effect is restricted to a small energy window around E_F, it can be quite dramatic: In three dimensions it is predicted to lead to a non-quasiparticle behaviour in the spectral function.[25]

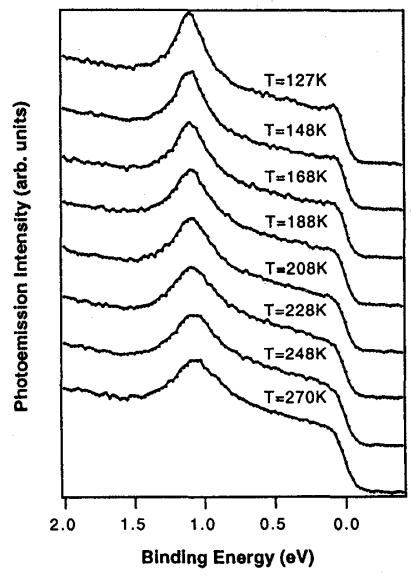

FIG. 6. Temperature dependence of the surface state linewidth near $\overline{C}$. $\hbar\omega = 16$ eV. From Ref. 24.

The (010) surface of α-gallium is a promising candidate for establishing an influence of the electron-phonon coupling on the dispersion of the electronic states. The size of the effect is given mainly by two factors: The phonon bandwidth E_{max} sets the energy scale and the so-called electron-phonon mass enhancement parameter λ determines the change in curvature of the dispersion at E_F. Both are relatively high in bulk α-Ga ($E_{max} = 40$ meV[26] and $\lambda = 0.98$[27]). An important practical requirement is that the surface should be atomically flat, because the small effect would otherwise be smeared out. This seems to be fulfilled in the case of the (010) surface of α-Ga as shown by the results of a scanning tunnelling microscopy study near its melting temperature (29.8 °C).[28,29] Finally, the surface has to support a surface state which crosses E_F. Such a state was predicted for α-Ga(010) in a recent first-principles calculation by Bernasconi, Chiarotti and Tosatti (BCT).[23] The state was found to form an electron pocket centered around the corner (the $\overline{C}$ point) of the surface Brillouin zone (SBZ) and to have a bandwidth of about 1.5 eV.

The predicted surface state at the $\overline{C}$ point was indeed found experimentally.[24] The surface state has been identified by the absence of dispersion with $k^{\perp}$, their sensitivity towards contamination and their position in gaps of the projected bulk band structure. We used the temperature dependence of its linewidth to determine the magnitude of the electron-phonon mass enhancement parameter λ at the surface following the example carefully illustrated by McDougall, Ba-

lasubramanian and Jensen for the Cu(111) surface state.[30] Fig. 6 shows the energy distribution curves of the surface state at $\overline{C}$ for temperatures between 127 and 270 K. Apart from the obvious broadening, the peak shifts slightly towards lower binding energies with increasing temperatures. Fig. 7 displays the Lorentzian width of the peak as a function of temperature. It was determined by fitting the peak with a Voigt line and a linear background. Assuming that the impurity scattering and Auger decay contributions to the hole lifetime are negligible, the temperature dependence of the linewidth can be calculated from the Eliashberg coupling function.[27] In the Debye model this temperature dependence is best fitted with a value of $\lambda = 1.4 \pm 0.10$ using $\omega_D = 28$ meV and $E_B = 1.1$ eV. Apparently the theoretical phonon contribution to the linewidth within the Debye model accounts for the entire experimental linewidth in the present case, which in turn suggests that the impurity scattering and Auger decay contributions to the life time are indeed very small. This indicates that the surface has very few defects, consistent with the STM results.[28] The electron-phonon coupling on this surface is very strong, even stronger than that for bulk α-gallium.

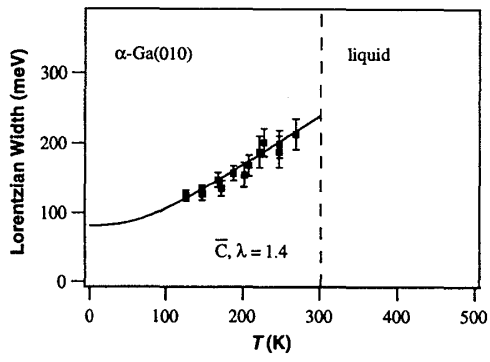

FIG. 7. Lorentzian contribution to the linewidth as a function of temperature. The error bars represent the uncertainties resulting from the fitting. The curve is a fit to the theoretical phonon contribution to the linewidth within the Debye model which yields $\lambda = 1.4 \pm 0.1$. From Ref. 24.

At 273 K a sharp (1×1) LEED pattern was observed. Every odd-integer spot in the [100] direction is missing, consistent with the glide-plane symmetry in bulk α-gallium. There are at least three different possible terminations for this surface, all of which are consistent with a glide-plane symmetry.[23] When the sample is cooled below about 220 K, the surface undergoes a phase transition in which the LEED pattern changes reversibly from (1×1) to $c(2\times2)$. The superstructure spots are weaker and less sharp than the (1×1) spots; spots can be observed at *all* integer positions which is compatible with the loss of the glide plane symmetry.

Fig. 8 shows the surface state dispersion at 273 and 120 K superimposed on the projected bulk band structure from BCT[23] as well as the SBZs for both phases. For both temperatures the surface state clearly runs into the bulk bands in the $\overline{C}-\overline{W}$ direction. In the $\overline{C}-\overline{\Gamma}$ direction the situation is somewhat unclear: The peak can no longer be observed beyond a certain point due to the vicinity of the intense and broad transitions from the bulk bands. The $\overline{C}-\overline{X}$ direction, however, shows pronounced differences between the high and the low temperature measurements. While the surface state crosses E_F in the former it does not reach it in the latter and, again, runs into the bulk bands instead. The smallest binding energy of the surface state peak is estimated to be about 120 meV.

Apart from this surface state band there is only one additional surface-related feature: Upon cooling a small peak can be observed very close to E_F in the immediate vicinity of $\overline{C}$. This feature is visible in Fig. 6 for the data taken at 127 K and is plotted in Fig. 8. When we try to fit the structure to determine its temperature dependence and dispersion, it is not possible to decide whether it disperses upwards and disappears, or whether it just broadens out as the separation from $\overline{C}$ increases or the temperature is raised. Hence, the weak dispersion indicated in Fig. 8 has been obtained only by fitting the peak with a fixed width and a variable energy position.

While our fits to the surface state peak suggest that the phase transition causes the opening of

a local band gap we have to be careful about such a statement. Indeed, all our data show a high background spectral intensity in the projected bulk band gap and our surface state to background ratio is significantly smaller than in other modern investigations of *sp*-derived surface states (see e.g. Ref. 30). A possible explanation for such a high background is defect-induced k-smearing. This, however, seems very unlikely in view of the measured surface state linewidth (see above) and the STM results. It seems more likely that the spectral intensity is due to a breakdown of the quasiparticle picture for this system. A non-quasiparticle behavior would in fact be expected because of the strong electron-phonon coupling in the present system.[25]

As for the nature of the phase transition, from our data it is not possible to determine whether the transition is a purely electronic long-range instability, i.e., a weak coupling charge density wave or caused by a short-range interaction.[31] The latter is more likely as this could explain a lower transition temperature than what the gap size would suggest if it was the former.[32] Furthermore, it would fit very well with the dangling bond character of the surface state at $\overline{C}$ suggested by BCT.[23] It seems likely that the surface gets rid of the dangling bonds by a dimerization of the surface atoms similar to the dimers in bulk α-Ga.

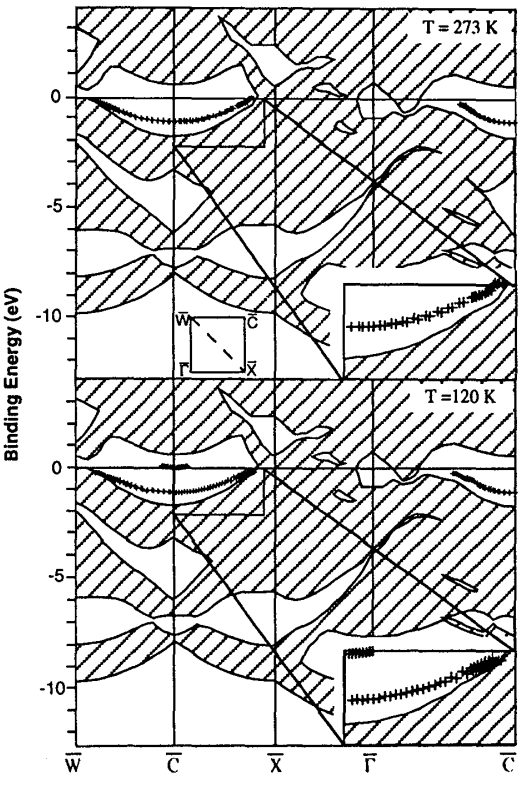

FIG. 8. Experimental surface state dispersion for $T = 273$ and 120 K, i.e. above and below, respectively, the (1×1) to c(2×2) phase transition. The projected bulk band structure has been taken from Ref. 23. The inset in the top part of the figure shows the irreducible part of the surface Brillouin zones for the (1×1) (solid) and c(2×2) (dashed) phase. From Ref. 24.

Apart from opening the gap the transition is accompanied by the new feature at $\overline{C}$. This could be simply a band just pulled close to E_F or it could be a direct manifestation of the new state in the spectral function. After all, it is found precisely at the new $\overline{\Gamma}$ point and only in a very narrow angular range. Note that there is no state at the $\overline{\Gamma}$ point which could be folded into the new one by the reconstruction.

ACKNOWLEDGMENTS

The author wishes to express his gratitude to the people with whom he has worked in the work presented here. In particular, M. Ritter, W. Weiss, and A. M. Bradshaw have made important contribution to the work on the iron oxide film, and Ph. Hofmann, Ch. Grütter, and J. H. Bilgram on the α-Ga(010). Ph. Hofmann has played a central role in the latter work.

[1] B. Feuerbacher, B. Fitton, and R. F. Willis, ed. *Photoemission and the Electronic Properties of Surfaces* (John Wiley & Sons, Chichester, 1978).
[2] C. Kunz, in Ref. 1, Chatper 17.
[3] See, e.g., S. Hüfner, *Photoelectron Spectroscopy: Principles and Applications* (Springer-Verlag, Berlin, 1995).
[4] S. F. Alvarado, W. Eib, F. Meier, H. C. Siegmann, and P. Zürcher, in Ref. 1, Chapter 15.
[5] V. E. Henrich and P. A. Cox, *The Surface Science of Metal Oxides* (Cambridge University Press: Cambridge, 1994).
[6] H.-J. Freund, H. Kuhlenbeck, and V. Staemmler, Rep. Prog. Phys. **59**, 283 (1996).
[7] W. Weiss, Surf. Sci. **377-379**, 943 (1997).
[8] N. Tsuda, K. Nasu, A. Yanase, and K. Siratori, *Electronic Conduction in Oxides* (Springer-Verlag: Berlin. 1991).
[9] M. Ritter, W. Ranke, and W. Weiss, Phys. Rev. B **57**, 7240 (1998).
[10] Th. Schedel-Niedrig, W. Weiss, and R. Schlögl, Phys. Rev. B **52**, 17449 (1995).
[11] W. Weiss, A. Barbieri, M. A. Van Hove, and G. A. Somorjai, Phys. Rev. Lett. **71**, 1848 (1993); A. Barbieri, W. Weiss, M.A. Van Hove and G.A. Somorjai, Surf. Sci. **302**, 259 (1994).
[12] E. J. W. Verwey and P. W. Haaymann, Physica **8**, 979 (1941); E. J. W. Verwey, P. W. Haayman, and F. C. Romeijn, J. Chem. Phys. **15**, 181 (1947).
[13] J. Yoshida and S. Iida, J. Phys. Soc. Jpn. **42**, 230 (1977); S. Iida, Philos. Mag. B **42**, 349 (1980).
[14] D. Ihle and B. Lorenz, Philos. Mag. B **42**, 337 (1980).
[15] Y. Q. Cai, M. Ritter, W. Weiss, and A. M. Bradshaw, Phys. Rev. B **58**, 5043 (1998).
[16] K. Siratori, S. Suga, M. Taniguchi, K. Soda, S. Kimura, and A. Yanase, J. Phys. Soc. Jpn. **55**, 690 (1986).
[17] R.J. Lad and V.E. Henrich, Phys. Rev. B **39**, 13479 (1989); and J. Vac. Sci. Technol. A **7**, 1893 (1989).
[18] A. Yanase and N. Hamada, unpublished; A. Yanase, ISSP Diaries **37**, 66 (1997) (in Japanese).
[19] S. F. Alvarado, W. Eib, F. Meier, D. T. Pierce, K. Sattler, and H. C. Siegmann, Phys. Rev. Lett. **34**, 319 (1975); S. F. Alvarado, M. Erbudak, and P. Munz, Phys. Rev. B **14**, 2740 (1976).
[20] A. Chainani, T. Yokoya, T. Morimoto, T. Takahashi, and S. Todo, Phys. Rev. B **51**, 17976 (1995).
[21] For a review, see, L.C. Davis, J. Appl. Phys. **59**, R25 (1986).
[22] Ph. Hofmann, R. Stumpf, V. M. Silkin, E. V. Chulkov and E. W. Plummer, Surf. Sci. **355**, L278 (1996).
[23] M. Bernasconi, G. L. Chiarotti and E. Tosatti, Phys. Rev. Lett. **70**, 3295 (1993); M. Bernasconi, G. L. Chiarotti and E. Tosatti, Phys. Rev. B **52**, 9999 (1995).
[24] Ph. Hofmann, Y. Q. Cai, Ch. Grütter and J. H. Bilgram, Phys. Rev. Lett. **81**, 1670 (1998).
[25] S. Engelsberg and J. R. Schrieffer, Phys. Rev. **131**, 993 (1963).
[26] W. B. Waeber, J. Phys. C **2**,903 (1969).
[27] G. Grimvall, *The Electron-Phonon Interaction in Metals* (North-Holland, New York, 1981).
[28] O. Züger and U. Dürig, Phys. Rev. B **46**, 7319 (1992).
[29] There exists some confusion as to the labelling of the axis in α-Ga. The notation used here is that defined in Landoldt-Börnstein, New series Vol. 6, eds. P. Eckerlin and H. Kandler, Heidelberg New York 1971. Our (010) surface corresponds to Züger and Dürig's (001) surface.
[30] B. A. McDougall, T. Balasubramnian and E. Jensen, Phys. Rev. B **51**, 13891 (1995).
[31] E. Tosatti in *Electronic Surface and Interface States on Metallic Systems* (eds. E. Bertel and M. Donath) World Scientific, Singapore (1995) and references therein.
[32] W. L. McMillan, Phys. Rev. B **16**,643 (1977).